A CFRP Belleville spring for a competition solar EV

Sizing, FEM verification and manufacture of a lightweight suspension element

Dejan Bekić | BSc Mechanical Engineering, University of Bologna | sole author, BSc thesis defended 24 March 2026

Scope. Independent academic project, developed entirely on my own outside any employment relationship and with academic resources only. It contains no confidential or proprietary information belonging to any organisation.

1. Application and design targets

The Onda Solare BWSC vehicle was weighed corner by corner; with a two-person crew the total mass is $m_{\text{tot}} = 700.8$ kg, with the design corner at 223.7 kg (front) and 138.9 kg (rear). The suspension offers only $s_{\max} = 20$ mm of travel, and the push-rod kinematic ratio is $\mu = 0.75$.

The travel budget fixes the ride frequency before any spring is chosen. The static sag associated with a natural frequency f_n is $\delta_{\text{stat}} = g/(2\pi f_n)^2$, so the travel constraint requires $f_n > 3.52$ Hz. The automotive default of 2.0 Hz would demand 62 mm of sag against 20 mm available and was discarded; $f_n = 4.0$ Hz gives 15.5 mm of sag and leaves 4.5 mm of bump margin. The resulting static spring load is 1756 N at the front corner and 1090 N at the rear.

Design quantity	Front	Rear	Unit
Corner mass, with crew	223.7	138.9	kg
Sprung mass per corner	134.2	83.3	kg
Static spring load	1756	1090	N
Peak bump load ($n_z = 2.5$)	4389	2725	N
Target spring rate	150.7	93.6	N/mm

Table 1: Design targets per corner. Sizing is carried out on the more heavily loaded wheel of each axle.

2. Why a disc spring, and why in CFRP

A helical coil compressed axially develops a lateral force and a torque, because the axial load acts on a lever arm with respect to the wire axis. Those parasitic loads are reacted by the damper rod, its seals and its bearings, where they show up as friction and wear. A Belleville (disc) spring flattens under load and produces no transverse component, which removes the loading path entirely.

The architecture brings two further properties that matter here. The force–deflection law is intrinsically non-linear, and its shape is governed by the height-to-thickness ratio h/t: below $h/t = \sqrt{2}$ the rate stays positive over the whole stroke, which is the regime selected. And the rate of a column is set by how the discs are stacked rather than by the disc itself, so the suspension can be re-rated without new tooling.

CFRP was then selected for the disc itself. The literature reports mass savings close to 80% against steel discs of equivalent characteristic (Dharan & Bauman 2007; Foard et al. 2019). On a solar vehicle, where unsprung mass feeds directly into both dynamic performance and energy consumption, that is the deciding argument.

3. Laminate, geometry and sizing

The disc is a 10-ply $[0/45/0/45/0]_S$ laminate in T300/epoxy 2×2 twill, 200 g/m^2, cured ply thickness 0.23 mm. Because the fabric is balanced, two cutting orientations cover all four canonical fibre directions; the stack is symmetric, so the membrane–bending coupling matrix $[B]$ vanishes and the plate does not warp coming off the mould. The in-plane response is quasi-isotropic, which is what licenses an isotropic-equivalent modulus in the analytical model.

Geometry			Equivalent properties		
Outer diameter D_e	74.0	mm	Flexural modulus $E_{1,\text{flex}}$	45 641	MPa
Inner diameter D_i	15.2	mm	Extensional modulus $E_{1,\text{ext}}$	43 953	MPa
Laminate thickness t	2.30	mm	In-plane shear G_{12}	12 947	MPa
Free cone height h	2.76	mm	Laminate density	1500	kg/m^3
Ratio h/t	1.20	–	Coupling matrix $[B]$	≈ 0	–
Ratio $\alpha = D_e/D_i$	4.87	–	Mass per disc	14.2	g

Table 2: Disc geometry and laminate constants. Stiffness terms computed ply-by-ply in ANSYS ACP from the measured lamina properties; the analytical model instead uses an isotropic equivalent, and the gap between the two is the subject of §4.

Sizing was implemented as a parametric MATLAB routine rather than as a one-off calculation: vehicle and material data go in, and the tool returns the equilibrium point, the force–deflection characteristic, the tangent rate, the disc count, the axial envelope, the mass and the inner-edge stress. Re-rating for a different platform is a matter of minutes.

Two points drove the numerical results. First, the tangent rate $dP/d\delta$, not the secant P/δ, sets the oscillation about the static equilibrium; using the secant would have overestimated the rate by 12% at the front and under-counted the discs in series. Second, with the equilibrium point at $\delta_{\text{eq}} = 0.325$ mm the disc operates in the stiffest part of its curve, which is why the column needs 33 discs at the front and 57 at the rear.

Sizing result	Front	Rear	Unit
Equilibrium deflection δ_{eq}	0.325	0.193	mm
Tangent rate of one disc	4828	5287	N/mm
Discs in series N_s	33	57	–
Resulting ride frequency f_n	3.94	3.98	Hz
Max deflection per disc at full bump	0.43	0.25	mm $(\delta/h \leq 0.16)$
Axial envelope of the column	167	288	mm
CFRP mass per corner	469	810	g
Disc mass, CFRP	469	810	g
Same discs in steel, for reference	2454	4239	g

Table 3: Analytical sizing output. The steel figure is the same disc geometry in steel, not an equivalent helical coil: no coil was sized in this work. Across four corners, 2.56 kg of CFRP against 13.39 kg of steel discs.

The analytical stress check did not close: at the front the inner-edge stress predicted by the closed-form model reaches 846 MPa against a laminate strength of 600 MPa. Rather than accept that as a design failure or dismiss it, it was treated as the question the FEM had to answer.

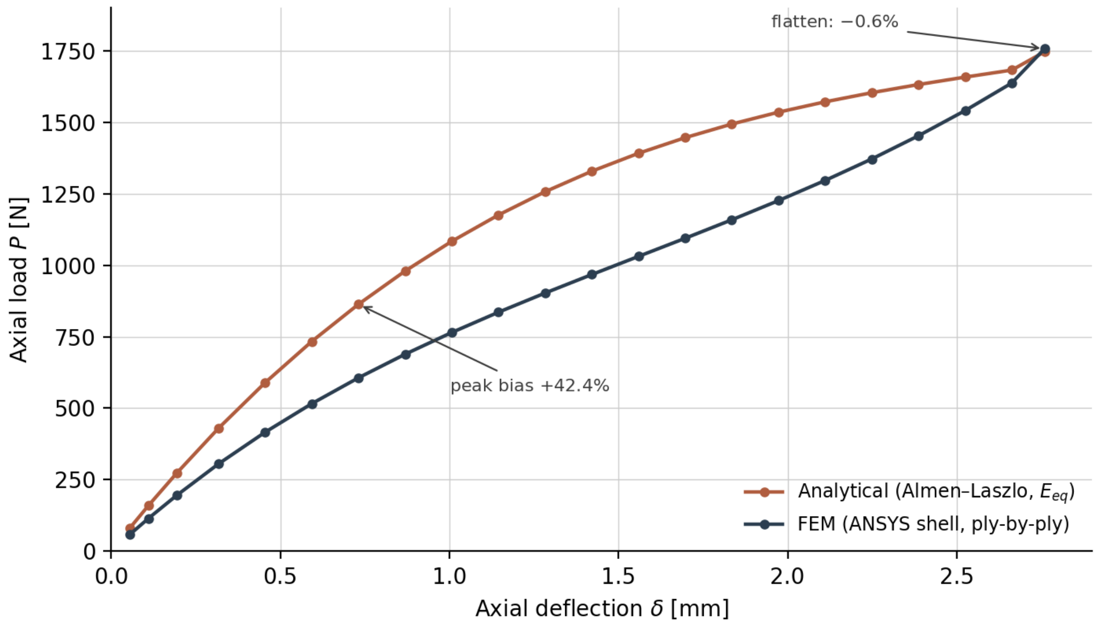

Figure 1: Axial force–deflection characteristic. FEM (ANSYS shell, ply-by-ply, geometric non-linearity) against the closed-form model with an isotropic-equivalent modulus. The two agree to −0.6% at full flatten; between 0.1 and 2.0 mm the closed form runs 25 to 42% high.

4. FEM verification

Since every disc of a series column carries the same axial force, verifying one disc verifies the column, and the saved budget was spent on mesh resolution instead. The model is a shell built in ANSYS ACP-Pre, justified by $t/a \approx 0.062$, with the full 10-ply layup encoded, fibre orientation assigned through a rosette centred on the disc axis, geometric non-linearity active, and Tsai–Wu as the failure criterion. The outer edge is axially restrained and the inner edge is displacement-driven to full flatten, which is what allows the whole characteristic to be traced rather than a single load point.

Where the models agree. At full flatten the FEM returns 1756.3 N against 1745.5 N analytical, a -0.6% gap. That is the check on geometry, boundary conditions and layup encoding.

Where they diverge, and why. Between 0.1 and 2.0 mm the closed form overpredicts the load by 25 to 42%, peaking at $+42.4\%$ near $\delta = 0.7$ mm. Two causes were identified. The isotropic-equivalent modulus averages away the circumferential variation of the flexural terms D_{11}, D_{22}, which is pronounced at $\alpha = 4.87$; and the rigid-section hypothesis degrades exactly where the flexural gradients concentrate, at the inner edge. The direction and magnitude match the band reported by Patangtalo et al. (2016) for quasi-isotropic composite discs and the initial softness measured by Foard et al. (2019).

What follows for the design. The bias is conservative: the real tangent rate is lower than predicted, so the disc count is if anything on the safe side, and no re-sizing was needed. The design margin was re-anchored to the FEM curve; the closed form was kept as a fast first pass, not as the verification of record.

Strength. The Tsai–Wu inverse reserve factor peaks at $\mathrm{IRF}_{\max} = 1.226$ in a very narrow band at the inner edge, with a laminate average of $\mathrm{IRF}_{\mathrm{avg}} = 0.273$. The peak is a singularity produced by the concentrated edge boundary condition, not a physical failure: in the assembly the load is transferred through a spacer over a finite contact ring. The laminate as a whole works at roughly 27% of capacity. This also resolves the analytical stress check of §3, and it is consistent with the radial fracture mode at the inner edge reported by Dharan & Bauman (2007).

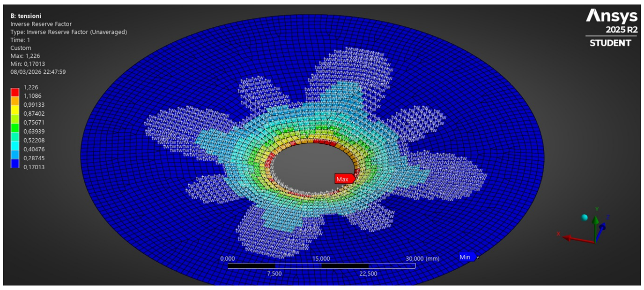

Figure 2: Tsai–Wu inverse reserve factor at design maximum deflection. The concentration governing failure sits at the ∅15.2 mm inner edge.

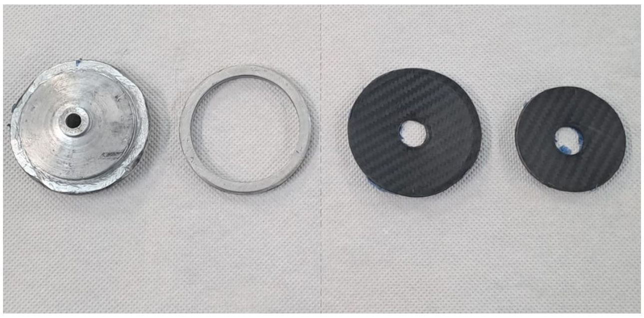

Figure 3: Self-produced CFRP discs alongside the matching tronco-conical moulds, CNC-machined in-house from the design drawings.

5. Manufacture, tolerances and assembly

The route was defined to be executable, and then executed. Ten prepreg annuli are cut oversize (+2 mm outer, −2 mm inner) to absorb fabric draw during conical forming and to leave stock for post-cure trimming, each one indexed against a fixed angular reference on the cutting template so the 0/45 sequence is actually the sequence in the part. Layup is by hand onto an aluminium mould released with a semi-permanent agent and a release film, compacted from the inner edge outwards, with an intermediate debulk at the mid-plane. Cure is 90 minutes at 120 °C under 0.5 MPa, with an 80 °C dwell to drop resin viscosity before gelation and demoulding held below 60 °C.

Drawings were issued to $\varnothing 74.00 \pm 0.10$ / $\varnothing 15.20 \pm 0.10$ / $t = 2.30 \pm 0.10$ mm, R_a 1.6 on the conical faces, with a datum scheme defined for stack assembly. DfM checks: single-sided tooling, no undercuts, demouldability verified, ply-drop strategy preserving symmetry. Machining is dry with PCD or coated carbide, since flood coolant would drive moisture into the matrix.

Quality control is per disc on dimensions, visual inspection under raking light, and mass against the 14.2 g nominal with a ±5% band; one disc in ten is compression-tested to flatten at 1 mm/min and compared against the predicted curve.

Two assembly details are not optional. PTFE spacers between discs in series eliminate the slip-stick behaviour that direct disc-on-disc contact produces, which would otherwise show up as step transitions in the rate curve; and a GFRP insulating layer breaks the CFRP-to-metal contact at the end plates, without which carbon and aluminium form a galvanic couple.

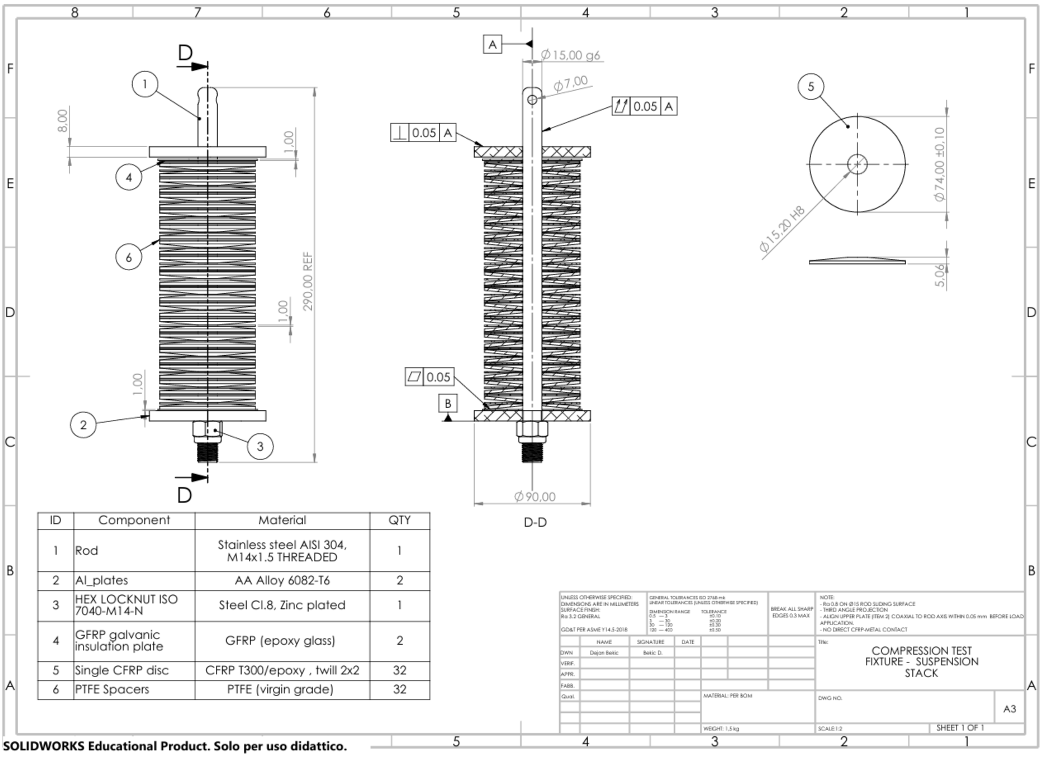

Figure 4: Assembly drawing of the bench-test fixture used to characterise the F–δ response of the stack under a uniaxial press: disc orientation, stacking order, end-cups and spacers. This is the laboratory test configuration; the on-car stack architecture, damper interface and preload strategy are covered in the full thesis.

6. Outcome

The spring meets the ride-frequency and travel targets at 3.94 and 3.98 Hz against a 4.0 Hz target, and stays within 16% of its flatten deflection at full bump. Strength is verified by FEM at 27% average laminate utilisation, with the inner-edge peak explained rather than absorbed into a safety factor.

On mass, the honest statement is narrow. Across four corners the discs weigh 2.56 kg in CFRP against 13.39 kg for the same geometry in steel. That ratio is the density ratio and nothing more: at fixed geometry no other number was available. No equivalent helical coil was sized, so this work carries no coil-versus-disc mass comparison, and the figure should not be read as one. What the architecture does buy, independently of mass, is the removal of the lateral load path into the damper seals and a rate that is re-tuned by changing the stack rather than the tooling.

The demonstrator uses CFRP for stiffness-to-mass, but the loop it exercises — requirements, closed-form model, parametric tool, FEM verification of the model's own assumptions, DfM-aware drawings, in-house fabrication — is agnostic to both material and component. The same sequence transfers to structural battery-pack mounts, drive-unit isolation, suspension links and BIW brackets, whether the answer turns out to be a CFRP layup, an aluminium stamping or a steel weldment.

Open items are stated as such: experimental validation on prototypes, cyclic fatigue characterisation, a parametric study on h, t and D_i to compress the axial envelope, and a full-stack model with contact to capture the friction effects a single-disc analysis cannot see.

References. [1] J. O. Almen, A. Laszlo, "The Uniform-Section Disc Spring," *Trans. ASME* 58, 305–314, 1936. [2] C. K. H. Dharan, J. A. Bauman, "Composite disc springs," *Composites: Part A* 38, 2511–2516, 2007. [3] J. H. D. Foard et al., "Polymer composite Belleville springs for an automotive application," *Composite Structures* 221, 110891, 2019. [4] W. Patangtalo, M. W. Hyer, S. Aimmanee, "On the non-axisymmetric behavior of quasi-isotropic woven fiber-reinforced composite Belleville springs," *J. Reinf. Plast. Compos.* 35(4), 334–344, 2016. [5] J. E. Shigley, C. R. Mischke, R. G. Budynas, *Mechanical Engineering Design*, 8th ed., McGraw-Hill, 2006.

Note. This document summarises a single-author BSc thesis (University of Bologna, defended 24 March 2026) covering the full Almen–Laszlo derivation, the MATLAB sizing tool, the ANSYS ACP setup, the stack-level architecture and the DfM iteration. Available on request.